Nanoscale Horizons

ROYAL SOCIETY OF CHEMISTRY

COMMUNICATION

View Article Online
View Journal

Cite this: DOI: 10.1039/d5nh00319a

Received 7th May 2025,
Accepted 18th June 2025

DOI: 10.1039/d5nh00319a

rsc.li/nanoscale-horizons

Unravelling quantum dot–molecule interactions for π-conjugated ligands: insights into binding and anchoring group effects†

Yinon Deree, Adar Levi, Xiang Li, Ori Gidron* and Uri Banin*

Quantum dots (QDs) coated with π-conjugated ligands display triplet energy transfer (TET), which opens the path for photon upconversion *via* QD photosensitization. Herein we study the effect of the ligand binding and its orientation on the triplet energy transfer efficiency through analysing the quenching of the QD photoluminescence. Comparing anthracene ligands with different anchoring groups, we find that replacing carboxylate with thiol or dithiol groups enhances quenching rates by factors of 3 and 4.5, respectively. To obtain this quantitative information, we devise a modified Stern–Volmer model taking into account the Poisson distribution of the ligand binding on the QDs. To this end, we show that bound anthracene-based ligands exhibit distinct spectral changes in their absorption spectra, including a ligand-dependent bathochromic shift with a modified vibronic progression and broadened spectral width. These changes, related to the deprotonation of the anchoring groups upon binding and the confined environment on the QD surface, enable the distinction of the crossover from bound to free ligands upon ligand addition. This allows us to incorporate accurate ligand binding stoichiometry to extract reliable quenching rates. Consistent with DFT calculations, the improved quenching for the thiolated anthracenes is ascribed to the parallel orientation of the π-system relative to the QD surface enabling larger orbital overlap that leads to faster TET rates *via* the Dexter mechanism. This work contributes to the design principles for efficient QD–organic hybrid systems towards improved triplet energy transfer.

New concepts

Hybrid systems composed of quantum dots (QDs) and π-conjugated organic ligands are widely used in optoelectronic and photochemical applications that rely on triplet energy transfer (TET). However, the design of such systems is hindered by the lack of reliable tools to quantify ligand binding, an essential parameter that governs energy transfer rates. Here, we introduce a novel optical method to quantify ligand binding to QDs, based on distinct and reproducible spectral changes in anthracene-based ligands with different anchoring groups. These changes enable accurate determination of ligand stoichiometry and are used to develop a modified Stern–Volmer analysis that accounts for ligand distribution. We show that thiolated ligands not only bind more effectively but also enhance quenching rates due to their favorable parallel π-system orientation relative to the QD surface, as supported by DFT calculations. This work establishes a new framework for quantitatively analyzing QD–ligand interactions and provides practical design principles for optimizing hybrid systems in photon upconversion and related applications.

Introduction

Hybrid systems composed of organic molecules and inorganic QDs play a crucial role in triplet energy transfer (TET)[1–3] and

Institute of Chemistry and the Center for Nanoscience and Nanotechnology, The Hebrew University, Jerusalem 91904, Israel. E-mail: ori.gidron@mail.huji.ac.il, uri.banin@mail.huji.ac.il

† Electronic supplementary information (ESI) available. See DOI: https://doi.org/10.1039/d5nh00319a

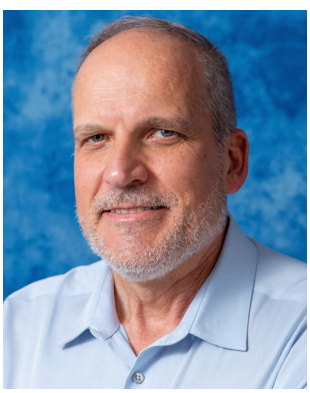

Uri Banin

Congratulations to the dedicated team at Nanoscale Horizons, as well as to its community of authors and readers, on the journal's 10th anniversary. In just a decade, Nanoscale Horizons has established itself as a leading platform for reporting breakthroughs and fostering critical dialogue in nanoscience. It has been an honor to serve on the journal's advisory board and a true pleasure to witness its growth and impact. Given the vibrant and evolving landscape of nanoscience across disciplines, I am confident that the journal's success will continue to flourish in earnest.

photoinduced electron transfer (PET),[4,5] two fundamental processes in various optoelectronic and photochemical applications. These processes are essential for technologies such as photocatalysis,[6,7] photochemistry,[6,8] photon upconversion,[9,10] and singlet fission,[11,12] where efficient energy and electron transfer are crucial for enhancing system performance. In such hybrid systems, π-conjugated ligands such as anthracene and tetracene carboxylic acid are frequently used, as their singlet and triplet energies are aligned with that of the QDs. Specifically, anthracene carboxylic acid (ACA) is considered a benchmark molecule in such hybrid systems.[1,3,13–15]

Along with matching the energy levels, an additional parameter concerns the orientation of the π-system relative to the QD surface that affects the QD–molecule orbital overlap. To this end, we compare anthracene ligands bearing carboxylate, thiol, and dithiol anchoring groups (ACA, TA, and DTA, respectively; Fig. 1a), which all lead to quenching of the QD photoluminescence (PL) upon binding, an indication of their functionality in TET. For analysis of the QD–ligand interaction, it is crucial to determine whether binding has occurred, as well as to quantify the number of bound ligands. Anthracene covalently bound to silicon QDs exhibits a red shift and broadening in its absorption spectrum,[16,17] attributed to electronic coupling. However, no spectral changes have been reported for carboxylate or thiol ligands bound to QDs. Therefore, the number of bound ligands is commonly approximated under the assumption that the extinction coefficient of the ligand does not change significantly upon binding, and that the absorbance originates from the bound ligand.[3,16–18] Deviations from one of these assumptions would lead to substantial errors in estimating the number of bound ligands per QD, and consequently, to substantial errors in estimating the TET rates.

Here we develop a modified Stern–Volmer (SV) equation that allows for extracting the quenching rate of a single bound ligand, taking into account the Poisson distribution of ligand binding. The analysis is based on our observation that binding the anthracene ligands leads to distinct spectral changes in their absorption spectra, including a ligand-dependent bathochromic shift with a modified vibronic progression and broadened spectral width. These spectral changes arise predominantly from the deprotonation of the anchoring group upon binding, with additional contributions from changes in the surrounding environment. These distinct changes serve as an indicator of ligand binding, enabling accurate quantification of the average number of ligands bound per QD. We find that replacing the carboxylic anchoring group with thiol or dithiol anthracene results in a 3 and 4.5-fold increase in the quenching rate, respectively. The enhanced quenching rate for the thiolated ligands is attributed to the parallel orientation of the π-system relative to the QD surface, enabling optimal orbital overlap, in agreement with DFT calculations. These findings facilitate the direct measurement of the QD ligand energy transfer process, providing further design principles towards the optimization of such hybrid systems.

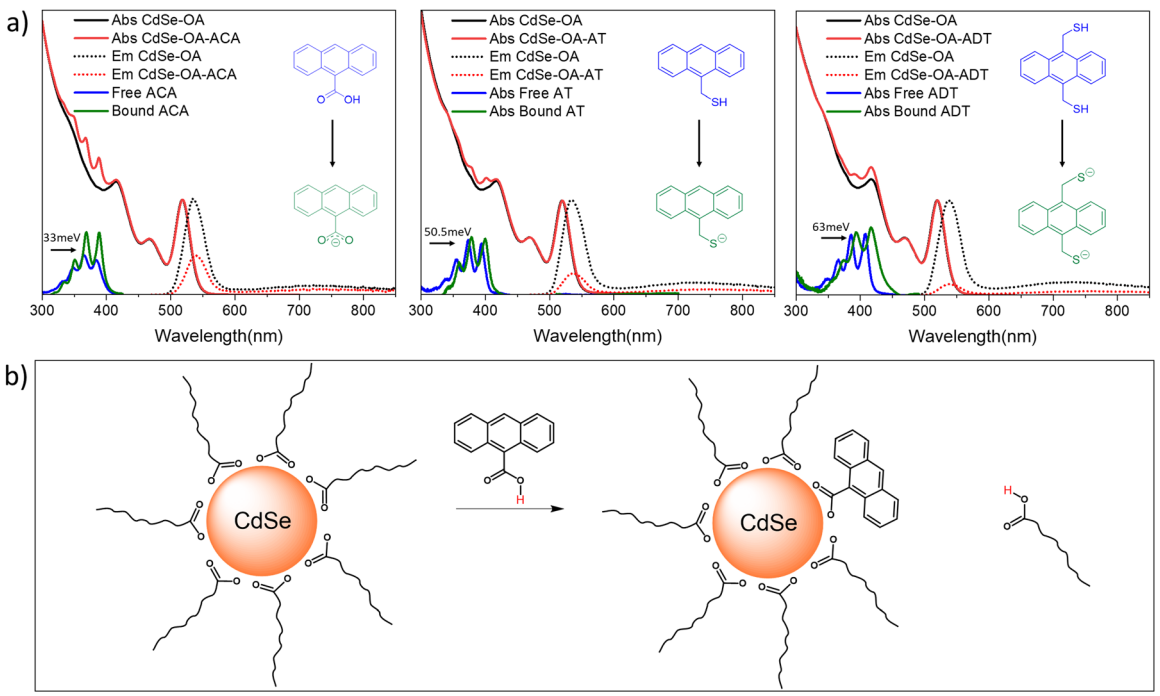

Fig. 1 (a) Normalized absorption (solid) and emission (dashed) spectra of CdSe–OA (CdSe QDs coated by oleic acid, black), free ligand (blue), CdSe–OA-ligand (red), and bound ligand (green). For each case, spectra are shown for ACA (anthracene carboxylic acid, left), AT (anthracene thiol, middle), and ADT (anthracene dithiol, right). The bound ligand spectrum was obtained by subtracting the absorption of CdSe–OA from that of CdSe–OA-ligand. The free and bound ligand spectra were measured at the same ligand concentration (equimolar solution), and the relative intensity ratio between them is preserved despite normalization. All spectra were recorded in toluene. The blue and green Lewis structures correspond to the ligands before and after binding, respectively. (b) ACA ligand exchange reaction with CdSe–OA, where there is proton exchange between OA^- and ACA.

Results and discussion

Upon adding 2 equivalents of the ligands to the CdSe QDs solution (2 equivalents correspond to an average of 2 ligands per QD, QD diameter 2.7 nm), significant PL quenching is observed, as reported in prior works for ACA (Fig. 1a). Remarkably, the thiolated ligands manifest a higher degree of quenching compared to the ACA, already pointing out the centrality of binding and ligand orientation in determining the TET efficiency. For quantitative information on the transfer rates, the dependence of the PL quenching on ligand coverage needs to be analysed. To this end, the first step is to quantify the degree of binding of the added ligands. Notably, we observe that the addition of ligands was also accompanied by a distinct shift of the absorption in the region of the ligands (Fig. 1a). This bathochromic shift depends on the ligand type, ranging from 33 meV for carboxylic bound ACA, to 50 meV for the AT that binds *via* a single thiol, to 63 meV for ADT with the two thiol groups. The bathochromic shift is accompanied by spectral broadening, most pronounced for ADT. The relative intensities of the vibronic peaks also change upon binding, which is related to the difference between ground and excited geometries. This difference is more pronounced for the thiolated ligands AT and ADT, as the 0–0 transition intensifies compared to the 0–1 and 0–2 transitions. This indicates a more rigid structure of the bound ligand compared to the free ligand. The bathochromic shift was also accompanied by a substantial increase in the extinction coefficient, as illustrated by the different intensities of equimolar solutions of free (blue) and bound (green) ligands in Fig. 1a. The increase in molar absorption coefficient is especially pronounced for ACA, with the bound ligand exhibiting nearly double the absorbance of the free ligand.

To explain the spectral changes upon binding, we measured the absorbance spectra of the deprotonated ligands using triethylamine and sodium methoxide as bases (Fig. S3–S5, ESI†). The spectral changes upon deprotonation correlate with the changes observed for the bound ligands. However, slight differences indicate that while deprotonation accounts for the major spectral changes observed upon binding, other factors, such as different chemical environments (Fig. S3–S5, ESI†) or electronic coupling, also contribute. Overall, binding affects the absorption spectra and the intensity of both the carboxylate and thiol ligands. An illustration of ACA binding to QD–OA is represented in Fig. 1b, where proton exchange takes place between OA^- and ACA.

To extract the quantitative quenching rates, we measured the emission and absorption upon the addition of ligands, as illustrated in Fig. 2 for ACA ligands added to CdSe–OA QDs. The red-shifted absorption, which is ascribed to the bound ligands, does not change upon adding the first 10 equivalents (Fig. 2a). The addition of more ACA ligands (>10 equivalents) results in a blue shift, indicating the presence of both bound and free ligands. This is clearly observed when plotting the lowest energy vibronic peak as a function of the ACA-to-QD ratio (Fig. 2b). Thus, there exists a regime where determining the

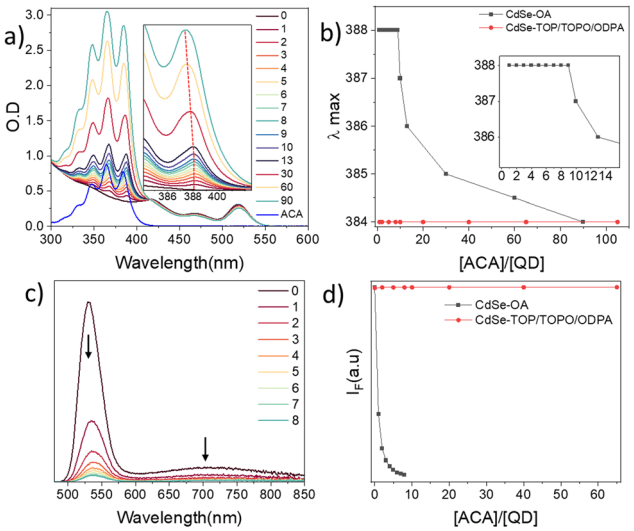

Fig. 2 (a) Absorption spectrum in various ACA to CdSe–OA ratios and only ACA (blue). Inset: At low ratios, all the ACA molecules bind to the QDs, as there is no change in the 388 nm peak position. The blue-shift observed above 10 equivalents of ACA indicates partial binding. (b) Lowest energy vibronic peak λ_{max} as a function of the ACA to QD ratio for CdSe–OA (black) and CdSe-TOP/TOPO/ODPA (red). (c) PL spectra of CdSe–OA in various ACA to CdSe–OA ratios, excited at 450 nm. (d) PL λ_{max} intensity as a function of the ACA to QDs ratio for CdSe–OA (black) and CdSe-TOP/TOPO/ODPA (red). All spectra were recorded in toluene. PL intensities are shown in arbitrary units (a.u.) representing relative counts.

average number of bound ligands is straightforward, being equal to the ligand-to-QD concentration ratio, as all ligands are bound under these conditions.

The binding also results in the quenching of the QD emission (Fig. 2c). Both the ligand spectral changes and the QD emission quenching were reversible upon the addition of OA, confirming that the binding of the labile ligand ACA is in equilibrium (Fig. S10 and S16, see ESI†). In contrast, starting from TOP/TOPO/ODPA ligands (TOP/O-trioctylphosphine/oxide; ODPA-octadecylphosphonic acid), which bind strongly to CdSe-QDs, no spectral change or emission quenching is observed, even upon addition of >60 equivalents of ACA (Fig. S17, see ESI†).[19] This confirms that TET requires direct ligand–QD surface binding, in line with the Dexter mechanism as previously reported.[3,18]

To understand why these spectral changes were previously overlooked, we need to consider the methods commonly used to prepare such hybrid systems: the most frequently applied preparation methods involve ligand replacement with a significant excess of ACA ligands, followed by the removal of any excess unbound ligands by washing.[3,18,20–23] We found that the washing process not only removes free ligands but also a portion of the bound ligands (Fig. S6, ESI†), inhibiting precise control and determination of the ligand coverage. The less commonly applied method is direct mixing, which involves ligand replacement without subsequent removal of free ligands.[14,15,24] We found that this method enables better monitoring of the binding process and that the binding occurs almost instantaneously without the need for prolonged heating

or sonication used in previous reports. At low ligand concentrations, nearly all the ligand molecules bind to the QD as confirmed by an equilibrium model (Fig. S1, see ESI†). This explains the absence of free ACA molecules below 10 equivalents. Since only 10 equivalents of ligands fully bind, the spectral changes are noticeable only at low ligand concentrations (Fig. 2a), which may explain why this phenomenon was previously overlooked.

Establishing the quantitative determination of the bound ligands allows us to introduce a model for extracting the quenching rates, which provides a measure of the TET processes. The SV equation, which addresses the effect of quenchers on the PL, is traditionally applied to molecules, not QDs, requiring further consideration. For instance, in the SV plot, the *x*-axis represents the concentration of the quencher, but this concentration is a less relevant variable for QDs. Instead, the average number of ligands bound to the QDs would be a more appropriate variable.

Additionally, SV analysis is typically used for two types of quenching mechanisms: dynamic and static. Dynamic quenching is unlikely, as collisions between the QDs and free molecules in solution do not typically quench the PL as observed above for the CdSe-TOP/TOPO/ODPA case. Instead, the quenching mechanism is static, *i.e.* between essentially bound anthracene ligands and the QDs.

Moreover, unlike molecules that undergo static quenching by forming a ground-state complex with a single quencher molecule, QDs can bind multiple quencher molecules. Furthermore, the extent to which a single ligand will quench the QD PL needs to be determined. If a single bound molecule were to completely turn off the emission of the QDs, the lifetime of the QDs should remain unaffected upon adding quenchers to the solution. This is because only the QDs without bound molecules would contribute to the signal, being the only ones capable of emitting light. However, as shown in Fig. 3a, the lifetime decreases with an increasing average number of ACA ligands bound to the QDs, indicating that a single molecule is not sufficient to cause complete quenching of the QDs PL.

This motivated us to introduce a modified SV model for hybrid QD–ligand systems. The model differs from previous models as it takes into account the observation that several quenchers are necessary for complete PL quenching in hybrid systems.[25,26]

To account for an average number of bound ligands, we assume a Poisson distribution of the ligands bound to the QDs (ESI† for further details). The quantum yield $\phi(n)$ of one QD with n ligands has the form:

$$\phi(n) = \frac{k_r}{k_r + k_{nr} + nk_q} \quad (1)$$

where k_r is the average QD radiative rate constant, k_{nr} is the average non-radiative rate constant and k_q is the quenching rate constant of a single molecule bound to the QD. Combining the Poisson distribution with eqn (1), we obtain $\bar{\phi}(x)$, the average quantum yield as a function of the average number of bound ligands $\left(x = \frac{[\text{Ligand}]}{[\text{QD}]}\right)$:

$$\bar{\phi}(x) = \sum_{n=1}^{\infty} p(n)\phi(n) = \sum_{n=1}^{\infty} \frac{x^n}{n!} e^{-x} \frac{k_r}{k_r + k_{nr} + nk_q} \quad (2)$$

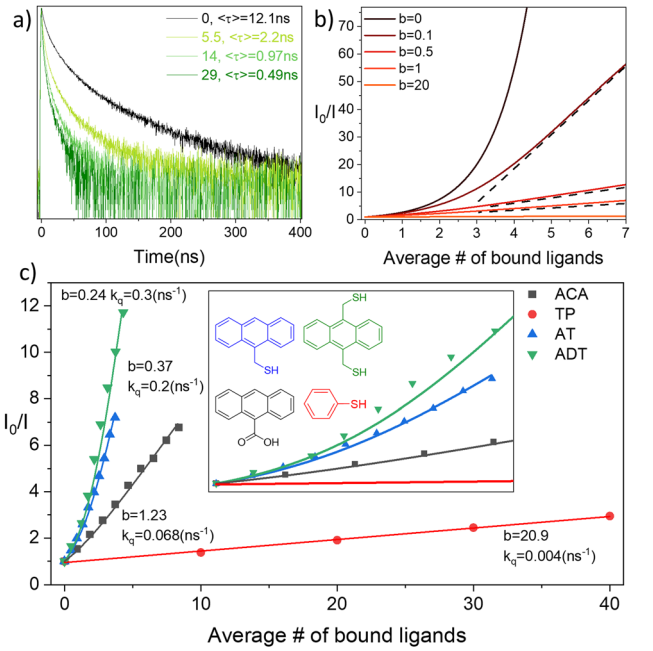

Fig. 3 (a) PL lifetime as a function of ACA : QD ratio in toluene is presented on a linear scale. (b) Plot of the SV model for different *b* values. (c) Stern–Volmer plot of CdSe–OA measured PL intensity ratios as a function of the average number for different bound ligands (symbols), along with the model fitting (solid lines). Inset: Expansion of the 0–5 equivalent region, with AT and ADT displaying exponential behaviour.

This form assumes that the quenching is additive, meaning that the overall quenching is the sum of the individual contributions of each bound ligand. Using all the above, we get an expression equivalent to the SV equation, for the experimentally determined $\frac{I_0}{I(x)}$ (for detailed derivation, see ESI†):

$$\frac{I_0}{I(x)} = \frac{b^{-1}}{\sum_{n=1}^{\infty} \frac{x^n}{n!} e^{-x} \frac{1}{b+n}} \quad (3)$$

where I_0 is emission intensity with no bound ligands, $I(x)$ is emission intensity with x the average bound ligands per QD and b is a parameter equal to the average decay rate constant of the QDs k_0 ($k_0 = k_r + k_{nr}$) divided by the quenching rate constant of a single bound molecule: $b = \frac{k_0}{k_q}$

We first examine this equation in two extreme limits: For $b \to 0$, which means that one bound ligand is sufficient for the complete quenching of the PL, eqn (3) converges to:

$$\frac{I_0}{I(x)} = e^x \quad (4)$$

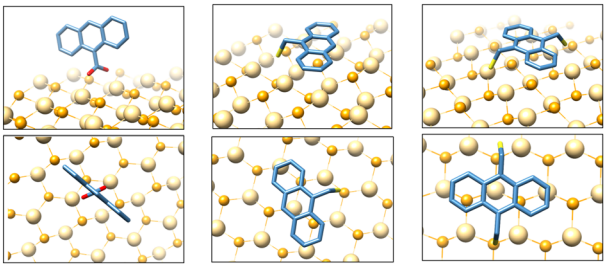

Fig. 4 Optimized structures of bound ligands are shown alongside illustrative binding orientations on the CdSe surface for ACA (left), AT (middle), and ADT (right). (a) Side view. (b) Top view.

In the other limit, if b is large, eqn (3) converges to the molecular Stern–Volmer equation $\left(\tau_0 = \frac{1}{k_0}\right)$, where the difference is that K^{SV} depends on the QD concentration $\left(K_{SV} = \frac{k_q \tau_0}{[QD]}\right)$:

$$\frac{I_0}{I(x)} = 1 + \frac{x}{b} = 1 + \frac{[\text{Ligand}]k_q\tau_0}{[QD]} = 1 + K_{SV}[\text{Ligand}] \qquad (5)$$

Fig. 3b presents a plot of the model with varying values of b. As b approaches zero, the exponential behavior becomes evident. Additionally, the plot shows convergence to linearity at high b values, or alternatively, as x increases, all the curves (for all b values) tend to linearity (Fig. 3b includes dashed-dot black lines representing the linear asymptote for the high x values). Two key insights can be drawn from this model:

(1) Strong quenchers (small b value) exhibit concave-up behaviour at small x values, and as the quencher strength increases (b approaching zero), the function exhibits full exponential behavior.

(2) The graph becomes linear for all x values in the limit of large b, with near-linear behavior already observed at $b = 1$. This indicates that when $k_q \sim k_0$ or when $k_q < k_0$ the graph is essentially linear.

Applying the model for studying the quenching rates of anthracene with a carboxylic anchoring group (ACA), and with one or two thiol anchoring groups (AT and ADT, respectively, Fig. 3c) reveals clearly the significant differences in their function and efficiency in TET. Since thiols were reported to quench the fluorescence by inducing traps, we also studied the quenching of thiophenol (TP) as a control.[27–29] The experiments were performed with ligand quantities ensuring that all ligands were bound to the QDs, as confirmed by the lack of any change in the bound ligand absorption spectrum (the "flat region" in Fig. 2b).

The SV plot in Fig. 3c displays a noticeable difference among the four ligands. The quenching rate of the thiol anthracene AT is 3 times faster than that of its carboxylic acid analogue ACA (0.07 ns^{-1} and 0.2 ns^{-1}, respectively), and the quenching rate of the dithiol ligand ADT (0.3 ns^{-1}) is 4.5 times faster than ACA. While ACA shows linear behavior, the thiol-anthracene ligands AT and ADT both exhibit exponential behavior, which the model predicts for the limit of strong quenchers (small b values). TP shows significantly slower rates (two orders of magnitude lower), confirming that the observed quenching for the anthracene ligands arises from TET processes, as previously reported for thiol-tetracenes[30] and also by upconversion experiments (Fig. S23, see ESI†).

Density functional theory (DFT) calculations can shed light on the observed differences in the quenching rates. While the frontier orbital energies do not differ significantly (Table S3, see ESI†), their orientation shows notable differences (Fig. 4). Since the carboxylate typically forms a bidentate bond on Cd surface sites,[31] ACA adopts a nearly orthogonal orientation (Fig. 4b, left), which should minimize the orbital interactions between the π-orbitals of the anthracene and the QDs. In contrast, the bond angles around the sulfur atom ($\sim 90^\circ$) are expected to result in a parallel orientation between the π-orbitals of the anthracene and the QD surface (Fig. 4b, middle and right). Since the TET rate is proportional to the orbital overlap between the QDs and ligands, this parallel orientation can explain the faster quenching observed for AT and ADT compared to ACA. The slightly faster quenching observed for the bidentate ADT compared with the monodentate AT could stem from a more stable parallel orientation of the former.

Conclusions

This work demonstrates that the binding of π-conjugated ligands to QDs can induce spectral changes, primarily due to the deprotonation of the anchoring group and changes in the surrounding environment. We show that these spectral changes, manifested as a redshift, line broadening and vibronic distortion, can serve as both quantitative and qualitative indicators of ligand binding, allowing us to determine the average number of bound ligands per QD directly. By using the average number of bound ligands, we developed a modified SV equation suitable for hybrid systems and applied it to compare different ligands. We find that while carboxylate ligands account for weaker quenching, corresponding to a linear SV behaviour, thiol anchoring groups account for stronger binding and exponential SV behaviour, explained by increased coupling in their parallel orientation. These findings establish a simple and effective optical approach to probe binding and electronic coupling at the ligand–QD interface to provide design principles for optimizing hybrid upconversion systems.

Author contributions

Conceptualization: Y. Deree, U. Banin, O. Gidron; methodology: Y. Deree, U. Banin, O. Gidron; investigation: X. Li, A. Levi (nanocrystal synthesis); Y. Deree (all other experiments); data curation: Y. Deree; writing – original draft: Y. Deree; writing – review & editing: Y. Deree, U. Banin, O. Gidron; supervision: U. Banin, O. Gidron; project administration and funding acquisition: U. Banin, O. Gidron.

Conflicts of interest

There are no conflicts to declare.

Data availability

All data supporting the findings of this study are included in the article and its ESI.†

Acknowledgements

U. B. acknowledges support from the Israel Science Foundation within the MAPATS program (Grant No. 2655/23) and thanks the Alfred & Erica Larisch Memorial Chair. OG acknowledges the European Union's Horizon 2020 research and innovation program (grant agreement no. 850836, ERC Starting Grant ''PolyHelix'') and the support of the Israel Science Foundation (grant No. 3085/21). Y. D. acknowledges the support from the Hebrew University Center for Nanoscience and Nanotechnology.

Notes and references

1 R. Lai, Y. Sang, Y. Zhao and K. Wu, *J. Am. Chem. Soc.*, 2020, **142**, 19825–19829.
2 T. Huang, S. He, A. Ni, T. Lian and M. Lee Tang, *Chem. Sci.*, 2024, **15**, 4556–4563.
3 C. Mongin, S. Garakyaraghi, N. Razgoniaeva, M. Zamkov and F. N. Castellano, *Science*, 2016, **351**, 369–372.
4 A. J. Morris-Cohen, K. O. Aruda, A. M. Rasmussen, G. Canzi, T. Seideman, C. P. Kubiak and E. A. Weiss, *Phys. Chem. Chem. Phys.*, 2012, **14**, 13794–13801.
5 S. Lian, D. J. Weinberg, R. D. Harris, M. S. Kodaimati and E. A. Weiss, *ACS Nano*, 2016, **10**, 6372–6382.
6 Y. Jiang, C. Wang, C. R. Rogers, M. S. Kodaimati and E. A. Weiss, *Nat. Chem.*, 2019, **11**, 1034–1040.
7 A. J. Bagnall, N. Eliasson, S. Hansson, M. Chavarot-Kerlidou, V. Artero, H. Tian and L. Hammarström, *ACS Catal.*, 2024, **14**, 4186–4201.
8 Y. Yuan, N. Jin, P. Saghy, L. Dube, H. Zhu and O. Chen, *J. Phys. Chem. Lett.*, 2021, **12**, 7180–7193.
9 Z. Huang, C.-H. Tung and L.-Z. Wu, *Acc. Mater. Res.*, 2024, **5**, 136–145.
10 Y. Niihori, T. Kosaka and Y. Negishi, *Mater. Horiz.*, 2024, **11**, 2304–2322.
11 J. Zhang, H. Sakai, K. Suzuki, T. Hasobe, N. V. Tkachenko, I.-Y. Chang, K. Hyeon-Deuk, H. Kaji, T. Teranishi and M. Sakamoto, *J. Am. Chem. Soc.*, 2021, **143**, 17388–17394.
12 C. Wang, M. S. Kodaimati, S. Lian and E. A. Weiss, *Faraday Discuss.*, 2019, **216**, 162–173.
13 Z. Chi, J. Xu, S. Luo, X. Ran, X. Wang, P. Liu, Y. He, Y. Kuang and L. Guo, *Phys. Chem. Chem. Phys.*, 2023, **25**, 8913–8920.
14 Z. A. VanOrman, C. R. I. Conti, G. F. Strouse and L. Nienhaus, *Chem. Mater.*, 2021, **33**, 452–458.
15 Z. A. VanOrman, A. S. Bieber, S. Wieghold and L. Nienhaus, *Chem. Mater.*, 2020, **32**, 4734–4742.
16 P. Xia, E. K. Raulerson, D. Coleman, C. S. Gerke, L. Mangolini, M. L. Tang and S. T. Roberts, *Nat. Chem.*, 2020, **12**, 137–144.
17 K. Wang, R. P. Cline, J. Schwan, J. M. Strain, S. T. Roberts, L. Mangolini, J. D. Eaves and M. L. Tang, *Nat. Chem.*, 2023, **15**, 1172–1178.
18 X. Li, Z. Huang, R. Zavala and M. L. Tang, *J. Phys. Chem. Lett.*, 2016, **7**, 1955–1959.
19 R. Gomes, A. Hassinen, A. Szczygiel, Q. Zhao, A. Vantomme, J. C. Martins and Z. Hens, *J. Phys. Chem. Lett.*, 2011, **2**, 145–152.
20 C. Mongin, P. Moroz, M. Zamkov and F. N. Castellano, *Nat. Chem.*, 2018, **10**, 225–230.
21 G. B. Piland, Z. Huang, M. Lee Tang and C. J. Bardeen, *J. Phys. Chem. C*, 2016, **120**, 5883–5889.
22 Z. Huang, X. Li, M. Mahboub, K. M. Hanson, V. M. Nichols, H. Le, M. L. Tang and C. J. Bardeen, *Nano Lett.*, 2015, **15**, 5552–5557.
23 Z. Huang, X. Li, B. D. Yip, J. M. Rubalcava, C. J. Bardeen and M. L. Tang, *Chem. Mater.*, 2015, **27**, 7503–7507.
24 L. Hou, A. Olesund, S. Thurakkal, X. Zhang and B. Albinsson, *Adv. Funct. Mater.*, 2021, **31**, 2106198.
25 A. M. Funston, J. J. Jasieniak and P. Mulvaney, *Adv. Mater.*, 2008, **20**, 4274–4280.
26 Z. A. VanOrman, R. Weiss, A. S. Bieber, B. Chen and L. Nienhaus, *Chem. Commun.*, 2023, **59**, 322–325.
27 G. Tang, X.-H. He, M. Liu, H. Hao, Y. Liu and F.-L. Jiang, *J. Phys. Chem. C*, 2024, **128**, 8681–8688.
28 G. Kalyuzhny and R. W. Murray, *J. Phys. Chem. B*, 2005, **109**, 7012–7021.
29 C. Bullen and P. Mulvaney, *Langmuir*, 2006, **22**, 3007–3013.
30 V. Gray, Z. Zhang, S. Dowland, J. R. Allardice, A. M. Alvertis, J. Xiao, N. C. Greenham, J. E. Anthony and A. Rao, *J. Phys. Chem. Lett.*, 2020, **11**, 7239–7244.
31 O. Voznyy, *J. Phys. Chem. C*, 2011, **115**, 15927–15932.

